Journal of Environmental Chemical Engineering 9 (2021) 106641

Contents lists available at ScienceDirect

Journal of Environmental Chemical Engineering

journal homepage: www.elsevier.com/locate/jece

Evaluation of nZVI for the degradation of atrazine in heterogeneous Fenton-like systems at circumneutral pH

Jorge Plaza [a], Amaya Arencibia [b], María José López-Muñoz [a,*]

[a] Department of Chemical and Environmental Technology, ESCET, Universidad Rey Juan Carlos, 28933, Móstoles, Madrid, Spain
[b] Department of Chemical, Energy, and Mechanical Technology, ESCET, Universidad Rey Juan Carlos, 28933, Móstoles, Madrid, Spain

ARTICLE INFO

Editor: Xianwei Liu

Keywords:
Zero-valent iron nanoparticles
Advanced oxidation processes
Fenton-like process
Water matrix
Atrazine degradation mechanism

ABSTRACT

The requirement of acidification for the successful of the Fenton processes in water treatment has promoted the search for new strategies to work at pH close to neutrality. With this objective, in this work the use of nZVI has been evaluated for the oxidative elimination of 10 mg L^{-1} of atrazine at circumneutral pH with nZVI/UVA, nZVI/H_2O_2, and nZVI/H_2O_2/UVA systems. While UVA irradiation of sole nZVI was ineffective for degrading the herbicide, the addition of H_2O_2 boosted up the reaction, with the nZVI/H_2O_2/UVA system attaining the highest degradation rate. The inhibition of the reaction upon addition of tert-butanol as scavenger pointed out the significant role of hydroxyl radicals in the atrazine oxidation. The characterization of fresh and spent samples, carried out by XRD, SEM, TEM, and nitrogen adsorption-desorption experiments, confirmed the presence of ferric oxidized compounds responsible of the heterogeneous photo-Fenton-like reactions. On the basis of the degradation products determined by high performance liquid chromatography (HPLC), a scheme of atrazine degradation pathways in the ZVI/H_2O_2/UVA system was proposed in which the reaction is mainly initiated by alkylic oxidation rather than dechlorination. Finally, the effect on the atrazine oxidation rate of the water constituent species was analyzed in different water matrices (pure, supply, simulated and secondary effluent real water). Considered individually, Cl^-, SO_4^{2-}, HCO_3^-, and DOC, showed a moderate inhibitory effect on atrazine degradation kinetics, but their combination could explain the significant decrease of efficiency detected in the real secondary effluent water compared to less complex matrices.

1. Introduction

Contamination of water resources with herbicides used in agriculture is a matter of great concern. As a result of the massive application of these compounds over years, they have become significant environmental pollutants, especially in aquatic ecosystems. Among high persistent herbicides, triazines represent an important group because they have been widely used for decades for selective broad-leaved and grassy weeds control on a variety of crops [1]. One representative member of triazines, likely the most widely used worldwide, is atrazine (2-chloro-4-ethylamino-6-isopropylamino-1,3,5-triazine). Its structure comprises a planar six-membered heterocyclic ring with three nitrogen atoms and three carbons ($C_3H_3N_3$) with high chemical stability. Atrazine has been classified as endocrine disruptor and is included in the list of priority substances of the European Union (Directive 2013/39/EU). Even though its application has been restricted or banned in many countries it is still detectable in surface and ground waters becoming an environmental concern [2].

Previous works have investigated the elimination of atrazine from aqueous systems through Fenton and photo-Fenton oxidation [3–5], reporting successful performances. As well known, the high efficiency of the Fenton process for the removal of pollutants in wastewater is based on the generation of reactive oxidizing species via the catalytic decomposition of H_2O_2 by ferrous ions (Fe^{2+}). The effectiveness of the process, however, is strongly dependent on pH, being necessary to operate in acidic conditions (optimum value at pH 2.8). As an example, Arnold et al. [3] reported a decrease of atrazine degradation by Fenton's reagent from 99% at pH 3 to 37% at pH 9, which was explained by the decrease of dissolved iron due to the formation of iron oxyhydroxides as the pH increased.

The requirement of an acidification pretreatment of polluted water, which also involves a neutralization of treated water before discharge, constitutes in addition to the buildup of iron sludge the main drawbacks of the classical Fenton reaction. To overcome these inconveniences, in

* Corresponding author at: Department of Chemical and Environmental Technology, ESCET, Universidad Rey Juan Carlos, 28933, Móstoles, Madrid, Spain.
E-mail addresses: jorge.plaza@urjc.es (J. Plaza), amaya.arencibia@urjc.es (A. Arencibia), mariajose.lopez@urjc.es (M.J. López-Muñoz).

https://doi.org/10.1016/j.jece.2021.106641
Received 8 June 2021; Received in revised form 17 September 2021; Accepted 20 October 2021
Available online 22 October 2021

the last years many efforts have been focused on developing strategies to effectively carry out Fenton processes at pH conditions close to neutrality using heterogeneous systems [6]. In them, Fe(III) species are mostly retained within the structure and in the pore-interlayer structure of the catalyst, hence $Fe(OH)_3$ precipitation is prevented while the catalyst keeps its ability to form $HO^{\bullet}$ by interaction with H_2O_2. In addition, the heterogeneous systems offer the advantage of an easy recovery of the solid catalyst at the end of reaction. Different solid iron catalysts have been investigated for Fenton-like oxidation processes, including zero-valent iron (Fe^0), and iron oxides and hydroxides such as hematite (α-Fe_2O_3) magnetite (Fe_3O_4), maghemite (γ-Fe_2O_3), wustite (FeO), goethite (α-FeOOH), or lepidocrocite (γ-FeOOH) [6,7]. Among them, one interesting proposal is the use of zero-valent iron (ZVI) since it has been demonstrated to be effective in treating various organic and inorganic pollutants [8]. In particular, special attention has been recently paid to zero-valent iron nanoparticles (nZVI) because of their small particle size and high superficial area that improve their surface reactivity compared to ZVI.

The present study aimed to evaluate the performance of nZVI for atrazine degradation at circumneutral pH under different reaction conditions, namely sole nZVI particles under UVA irradiation (nZVI/UVA), nZVI and hydrogen peroxide (nZVI/H_2O_2), and nZVI and H_2O_2 under UVA irradiation (nZVI/H_2O_2/UVA). A mechanism for atrazine degradation with nZVI was proposed, based on the intermediate products detected by high performance liquid chromatography (HPLC). Finally, the influence of the water matrix on the efficiency of the reaction was evaluated comparing ultrapure water, public supply water, simulated, and secondary effluent of a sewage treatment plant, to elucidate the individual effect of each major species usually present in non-ultrapure aqueous matrices.

2. Materials and methods

2.1. Chemicals

All chemicals were used as received without further purification. Atrazine 99% (2-chloro-4-ethylamino-6-isopropylaminos-triazine), desisopropyl-atrazine 95% (2-chloro-4-ethylamino-6-amino-striazine), desethyl-atrazine 99% (2-chloro-4-amino-6-isopropylamino-s-triazine), hydroxy-atrazine 96% (2-hydroxy-4-ethylamino-6-isopropylamino-s-triazine), desisopropyl-2-hydroxyatrazine 95% (2-hydroxy-4-ethylamino-6-amino-s-triazine), desethyl-2-hydroxy-atrazine 99% (2-hydroxy-4-amino-6-isopropylamino-s-triazine), desethyl-desisopropyl-atrazine 95% (2-chloro-4,6-diaminos-triazine), ammeline 95% (2-hydroxy-4,6-diamino-1,3,5-triazine), ammelide 99% (2,4- dihydroxy-6-amino-1,3,5-triazine), cyanuric acid 98% (2,4,6-trihydroxy-s-triazine) and hydrogen peroxide (H_2O_2, 30% in water) were purchased from Sigma-Aldrich. Hydrochloric acid (HCl) and sodium hydroxide (NaOH), used to adjust the pH value of the solutions, sulfate heptahydrate ($FeSO_4{\cdot}7H_2O$; > 99%), ethanol (99.7%), sodium borohydride ($NaBH_4$; > 98%), o-phenanthroline, anhydrous sodium acetate, acetic acid, sodium phosphate monobasic (NaH_2PO_4), sodium phosphate dibasic (Na_2HPO_4) and acetonitrile (HPLC grade) were supplied by Scharlab. The chemical solutions were initially prepared in deionized water (18.2 MΩ Milli-Q®). To study the influence of water matrix in the atrazine degradation, the following water matrices were also evaluated: i) Public water (PW) obtained from the local drinking water supply; ii) secondary effluent (RW) collected at a sewage treatment plant located in Móstoles (Madrid, Spain). The grab sample was stored in the dark at 4 °C and tested within 10 days after sampling; and iii) synthetic secondary effluent (SW), which was prepared according to [9].

2.2. Synthesis of nZVI particles

The nZVI particles were prepared by a modified method based on Ref. [10]. Briefly, 10 g of $FeSO_4{\cdot}7H_2O$ were dispersed in 200 mL of a mixture containing ultrapure water and ethanol (70:30 v/v) and sonicated for 2 h until a clear solution was observed. The ferrous solution was stirred under nitrogen while the pH was adjusted to 6.8 by NaOH addition. Then $NaBH_4$ powder was gradually added to the mixture in 10% excess over the stoichiometric amount, thus leading to the precipitation of zero valent iron nanoparticles. After separation by filtration, nanoparticles were washed with pure ethanol three times, dried under vacuum overnight at 80 °C, and stored in nitrogen atmosphere.

2.3. Photocatalytic reactions

The reactions were performed in a 1 L batch reactor with continuous air flow (0.1 L min^{-1}) and orbital stirring. The reactor was axially irradiated by an immersed medium-pressure mercury lamp (Heraeus TQ-150) placed inside a double Pyrex jacket through which an aqueous solution of copper sulfate (0.01 M) was circulated to prevent the overheating of the solution and to cut off the radiation below 300 nm. In all experiments an initial concentration of 10 mg L^{-1} was set for atrazine and 0.1 g L^{-1} for the nZVI. For Fenton reactions, the initial concentration of hydrogen peroxide was set to at 50 mg L^{-1}. Aliquots taken over reaction time were diluted with acetonitrile in a volume ratio 10:1 and filtered through a 0.22 μm syringe-driven Nylon filter prior to analysis. Acetonitrile was added to prevent Fenton and Fenton-like reactions to continue and to draw out any trace of atrazine or derivatives that might be trapped in the filter.

2.4. Analytical methods

Total dissolved iron and ferrous iron concentrations were determined by colorimetry at 510 nm according to the o-phenanthroline method (ISO 6332). Hydrogen peroxide was analyzed at 410 nm using titanium(IV) oxysulfate solution (DIN 38 402 H15). Both measurements were carried out using a JASCO V-630 spectrometer. The quantification of anionic species in the different aqueous matrices was performed by ionic chromatography (Metrohm Compact IC Flex). Dissolved organic carbon (DOC) was analyzed by a Shimadzu model TOC-V CSH apparatus. A High-Performance Liquid Chromatography system equipped with DAD detector (Agilent 1260 Infinity II) and a Poroshell 120 EC-C18 column was used to identify and quantify the atrazine and the main intermediates obtained along the reactions. Atrazine, desethyl-atrazine and desisopropyl-atrazine were eluted with a gradient of aqueous phosphate buffer (pH 7)-acetonitrile (55:45, v/v) to (35:65, v/v), at a flow rate of 1 mL min^{-1} and detected at 210 nm. All the other components of the reaction mixture were determined by a gradient elution with phosphoric acid buffer (pH = 3)-acetonitrile (95:5, v/v) to (40:60, v/v), at a flow rate of 0.8 mL min^{-1} and UV detection at 205 nm and 190 nm.

X-Ray Diffraction (XRD) patterns were acquired using Philips X-PERT MPD equipment with Cu Kα radiation (λ = 1.5414 Å) as X-ray source. Data were recorded in the range 10–80° at a 0.01° step size. The morphology of the synthesized nZVI particles was observed by scanning electron microscopy (SEM) (Philips XL30 ESEM) at operating voltage of 20 kV and transmission electron microscopy (TEM) (JEOL JEM 2100) with an acceleration voltage of 200 kV and a resolution between points of 0.25 nm. The adsorption-desorption isotherms were determined (Micromeritics Tristar 3000) using N_2 at 77 K. Previously to the analysis, the samples were subjected to two degasification steps under nitrogen at 363 K and 473 K for 5 h. BET surface area (S_{BET}) was determined using adsorption data in the relative pressure (P/P_0) between 0.05 and 0.2.

3. Results and discussion

3.1. Evaluation of nZVI activity for atrazine degradation

A preliminary experiment was carried out at natural pH (≈ 6.3) with atrazine at 10 mg L^{-1} to evaluate the performance of bare nZVI in dark conditions. The concentration of atrazine remained constant in the

solution after 120 min, thus indicating both a negligible adsorption of the herbicide on the nZVI surface and the absence of redox reactions.

Fig. 1a shows the concentration profiles of the reactions carried out with nZVI under UVA irradiation. As can be observed no significant activity for atrazine removal was detected either at the natural pH value of atrazine or at a pH close to that usually found in real secondary effluents of sewage treatment plant (pH ≈ 8). Conversely, the complete degradation of atrazine was attained at pH = 3 within 60 min of irradiation.

The distinctive efficiency observed at pH = 3 can be explained by the aerobic corrosion of metallic iron particles in the aqueous solution at acidic pH, which results in the formation of Fe^{2+} ions and the in situ production of H_2O_2 [11–14]. Two different mechanisms have been proposed to explain it: i) a two-electron transfer reaction between metallic iron and oxygen to yield H_2O_2 and ferrous ions (Eq. (1)); and ii) a series of one-electron transfer reactions between Fe^{2+} and oxygen to eventually produce hydrogen peroxide (Eqs. (2) and (3)):

$$Fe^0 + O_2 + 2H^+ \rightarrow Fe^{2+} + H_2O_2 \quad (1)$$

$$Fe^{2+} + O_2 \rightarrow Fe^{3+} + O_2^{\bullet -} \quad (2)$$

$$Fe^{2+} + O_2^{\bullet -} + 2H^+ \rightarrow Fe^{3+} + H_2O_2 \quad (3)$$

In addition to the acidic corrosion the irradiation of iron particles may also promote the oxidation of Fe(0) to ferrous ions (Eq. (4)) [15, 16]:

$$Fe^0 + h\nu \rightarrow Fe^{2+} + 2e^- \ (< 400\ nm) \quad (4)$$

Once ferrous ions and H_2O_2 are produced, the Fenton reaction would be triggered with the subsequent formation of oxidizing reactive species (Eqs. (5) and (6)), leading to the degradation of atrazine [11]:

$$Fe^{2+} + H_2O_2 \rightarrow Fe^{3+} + HO^- + HO^{\bullet} \quad (5)$$

$$Fe^{3+} + H_2O_2 \rightarrow Fe^{2+} + HO_2^{\bullet} + H^+ \quad (6)$$

The in situ generation of H_2O_2 was probed by quantifying its concentration in the solution after 2 h in the reaction of nZVI at pH = 3 under UV irradiation. The amount detected following the DIN 38 402 H15 method was 15 μM H_2O_2 (0.51 mg L^{-1}), value similar to that reported in previous works and considered as the excess of H_2O_2 not directly consumed in the reaction [11,17]. In addition, the HPLC analysis of aliquots taken along the irradiation time confirmed the presence of products usually found in the oxidative degradation of atrazine, among which 4-amino-2-chloro-6-isopropylamino-1,3,5-triazine (ACIT) and 6-amino-2-chloro-4-ethylamino-1,3,5-triazine (ACET).

On the contrary, if the corrosion of nZVI is prevented or delayed, as expected under circumneutral pH conditions at the time scale investigated, a significant drop in the activity for atrazine depletion will occur unless there is a removal mechanism alternative to the Fenton reaction. Most studies found in the literature about the use of bare nZVI particles at different pH are focused on the decolorization and total organic carbon (TOC) removal of dyes in solution. Four potential mechanisms, i.e. reduction, oxidative degradation, coagulation/precipitation and adsorption are considered responsible for the activity of nZVI particles, being their contribution highly dependent on the pH conditions [18]. As an example, Fujioka et al. [19] investigated the removal of Orange II by nZVI in the pH range 3–9. Besides the successful decolorization of the dye solutions, they reported an increase of the TOC removal from 10% to 40% by increasing the pH from 3 to 9, respectively. The results obtained were explained by means of the adsorption of Orange II and its intermediates on the iron oxide/hydroxides formed on the nZVI surface and a likely coagulation/sedimentation mechanism at the higher pH. None of the latter mechanisms is, however, effective for atrazine removal by the sole nZVI particles as the results shown in Fig. 1a indicate, which led to discard the application of bare nZVI for atrazine treatment at circumneutral pH.

The activity of nZVI was next examined by adding H_2O_2 in dark conditions and under UVA irradiation, i.e., in Fenton and photo-Fenton-like processes (nZVI/H_2O_2 and nZVI/H_2O_2/UVA, respectively). Fig. 1b shows that, in contrast to the negligible activity observed in the nZVI/UVA system at near neutral pH, the addition of H_2O_2 caused a substantial improvement in atrazine elimination, attaining after 120 min ca. 50% removal (nZVI/H_2O_2), which was further increased to 80% by UVA irradiation. It is worthy to note the different atrazine concentration profiles with time observed in the two reaction systems. In the nZVI/H_2O_2 system, it is detected a two-stage kinetics composed of an initial phase with a fast degradation of atrazine, followed by a marked slowdown of the reaction rate in a second stage. By contrast, in the nZVI/H_2O_2/UVA system the kinetics of the reaction followed a pseudo-first order decay with a $k_{obs} = 1.7 \cdot 10^{-2}$ min^{-1}. The content of total iron in solution was determined along the reaction in both systems. Concentrations of 1.8 and 1.0 mg L^{-1} were obtained at the end of the reactions with nZVI/H_2O_2 system and nZVI/H_2O_2/UVA, respectively, indicating the major contribution of the heterogeneous reaction at the nZVI surface, in contrast to the homogeneous reaction involving released iron ions, more likely at acidic pH.

The different H_2O_2 consumption and activity for atrazine degradation observed between nZVI/H_2O_2 and nZVI/H_2O_2/UVA systems indicates that nZVI particles are moderately reactive to H_2O_2 in the dark, being necessary the contemporary irradiation of the system to boost the

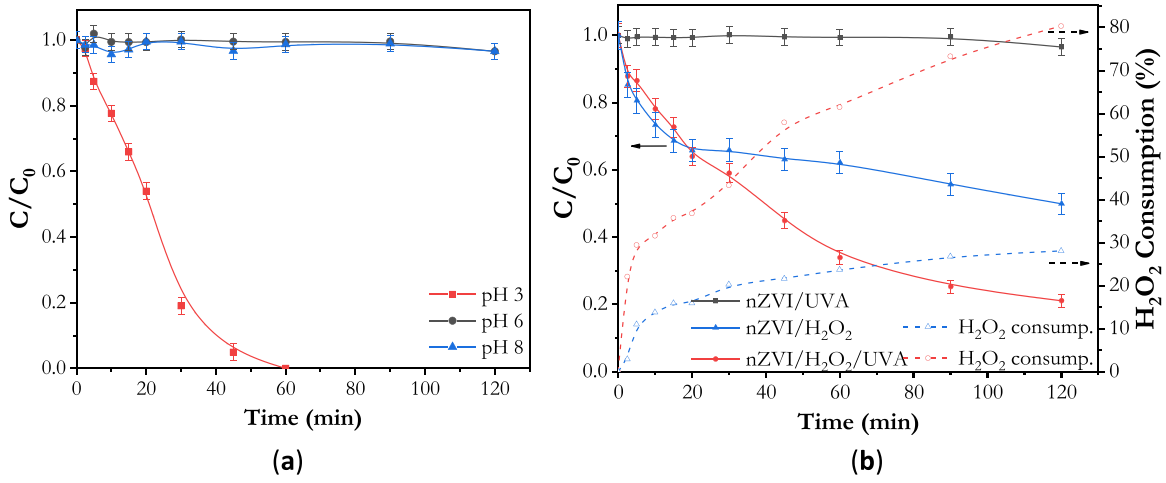

Fig. 1. (a) Influence of pH on the concentration profiles of atrazine with time in the nZVI/UVA system; (b) Atrazine degradation at pH ≈ 6.3 in the nZVI/UVA, nZVI/H_2O_2 and nZVI/H_2O_2/UVA systems. Experimental conditions: $[ATZ]_0 = 10$ mg L^{-1}; $C_{nZVI} = 0.1$ g L^{-1}; $[H_2O_2]_0 = 50$ mg L^{-1}.

reaction. Whereas the corrosion of nZVI is enhanced at low pH (Eq. (1)), it has been reported that the surface of the particles is passivated at higher pH through the formation of iron oxides/hydroxides [18]. Their presence was corroborated by the characterization of the nZVI particles by XRD and electron microscopy (shown in the next section). Therefore, the results obtained at pH 6.3 can be rationalized by considering the presence on the nZVI surface particles of Fe(III) and Fe(II) species able to react with H_2O_2 to yield oxidant species (Eqs. (7) and (8)). The increase of the reaction rate observed in the nZVI/H_2O_2/UVA system in comparison to nZVI/H_2O_2 can be ascribed to the reduction of Fe(III) into Fe (II) species promoted by the UVA irradiation (Eq. (9)) and the photo-Fenton-like reaction [20,21]:

$$\equiv Fe^{III}\text{-}OH + H_2O_2 \rightarrow \equiv Fe^{II} + HO_2^{\bullet} + H_2O \quad (7)$$

$$\equiv Fe^{II} + H_2O_2 \rightarrow \equiv Fe^{III}\text{-}OH + HO^{\bullet} \quad (8)$$

$$\equiv Fe^{III}\text{-}OH + h\nu \rightarrow \equiv Fe^{II} + HO^{\bullet} \quad (9)$$

The increase of Fe(II) species, able to undergo a reaction with H_2O_2 much faster than ferric species, would therefore accelerate the consumption of H_2O_2 and the rate of reaction. In agreement, Fig. 1b shows the enhancement of H_2O_2 consumption at the end of the reaction from 30% in nZVI/H_2O_2 to 80% in the nZVI/H_2O_2/UVA system. On the other hand, as Fe(II) regeneration is the rate determining step of the Fenton reaction [21], a limited number of $\equiv Fe^{II}$ species in the nZVI/H_2O_2 system, not easily regenerated from $\equiv Fe^{III}$ in the absence of irradiation, would explain the slowdown of the reaction rate observed after 20 min (Fig. 1b).

As an alternative to Eqs. (7)–(9), previous studies focused on iron oxides as heterogeneous catalysts in Fenton-like processes have proposed the generation of hydroxyl radicals through either, a chain mechanism initiated by the formation of an inner-sphere complex between H_2O_2 and surface $\equiv Fe^{III}$-OH [22], or by a non-radical mechanism in which the adsorbed substrate and H_2O_2 react on the catalyst surface [23]. Nevertheless, there is no agreement in the literature about the oxidation mechanism in Fenton-like heterogeneous systems, as not only $HO^{\bullet}$ but Fe(IV) species or even both have been suggested as major oxidant species responsible for the degradation of organic molecules. Hug and Leupin [13] and Keenan and Sedlak [14] proposed that the nature of oxidants is determined by pH, being $HO^{\bullet}$ predominant at pH values below 5 while different species such as Ferryl ion Fe(IV) are the main oxidants at higher pH values. He et al. [24] suggested a different mechanism to explain the degradation of the dye MY10 by heterogeneous photo-Fenton reaction in aqueous dispersions of α-Fe_2O_3, α-FeOOH, and β-FeOOH at neutral pH, which could be also considered for passivated nZVI. They proposed the initial formation of a surface $\equiv Fe^{III}OOH$ complex by the interaction of H_2O_2 with surface metal centers (Eq. (10)). Under UV irradiation, the complex would be broken to yield $HO^{\bullet}$ and $\equiv Fe^{IV}=O$ species, which are very unstable and react instantly with water to form more $HO^{\bullet}$ radicals (Eqs. (11) and (12)).

$$\equiv Fe^{III}\text{-}OH + H_2O_2 \rightarrow \equiv Fe^{III}OOH + H_2O \quad (10)$$

$$\equiv Fe^{III}\text{-}OOH + h\nu \rightarrow \equiv Fe^{IV}=O + HO^{\bullet} \quad (11)$$

$$\equiv Fe^{IV}=O + H_2O \rightarrow \equiv Fe^{III}OH + HO^{\bullet} \quad (12)$$

According to this mechanism, the increase of the reaction rate for atrazine degradation by UVA irradiation at circumneutral pH (nZVI/H_2O_2/UVA system) would be mainly due to the improved formation of $HO^{\bullet}$ through Eqs. (11) and (12).

To get some information about the contribution of $HO^{\bullet}$ radicals as oxidizing agents involved in the reaction of atrazine degradation with nZVI/H_2O_2/UVA, a series of experiments with a selective quencher, tert-butanol (t-BOH), were carried out (Fig. 2). t-BOH is known as an efficient $HO^{\bullet}$ scavenger through Eq. (13) ($k_{t\text{-}BOH/OH} = 3.8–7.6{\cdot}10^8\ M^{-1}\ s^{-1}$) [25].

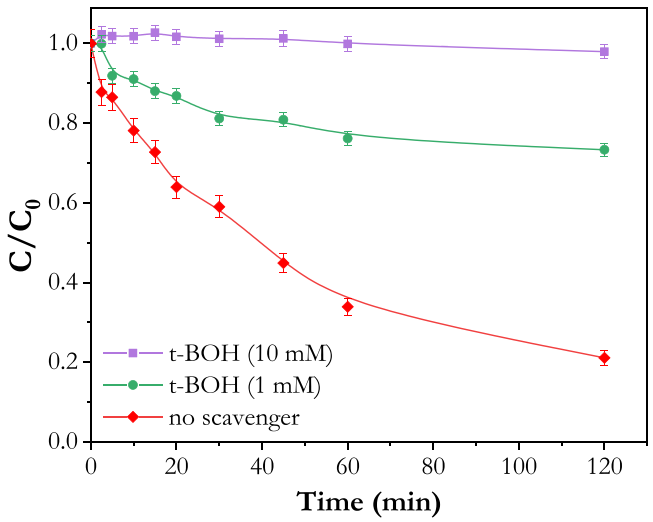

Fig. 2. Effect of t-BOH on the degradation of atrazine in the nZVI/H_2O_2/UVA system. Experimental conditions: $[ATZ]_0 = 10\ mg\ L^{-1}$; $C_{nZVI} = 0.1\ g\ L^{-1}$; $[H_2O_2]_0 = 50\ mg\ L^{-1}$; pH ≈ 6.3.

$$t\text{-}BOH + HO^{\bullet} \rightarrow t\text{-}BO^{\bullet} + H_2O \quad (13)$$

The presence of 1 mM of t-BOH led to a significant suppression of atrazine degradation (around 75%), with a decrease of the kinetic constant from 0.0114 to 0.0034 min^{-1}. The increase of t-BOH concentration to 10 mM completely inhibited the reaction indicating the preeminent role of $HO^{\bullet}$ in the atrazine oxidation mechanism.

3.2. Characterization of iron nanoparticles

The analysis of the iron nanoparticles was carried out by XRD, SEM and TEM in order to get information about the influence of reaction conditions on the formation of iron corrosion products.

Fig. 3 displays the XRD patterns of fresh and spent nZVI. Fresh iron nanoparticles showed the three characteristic peaks at $2\Theta = 44.4°$, 64.5° and 81.6° indexed, respectively, to (110), (200) and (211) reflections of metallic iron, α-Fe, (JCPDS, No. 01-085-1410). The latter is the main component of the particles, although it is also observed a broad peak at around 35° which can be related to the mild presence of iron oxide species, such as hematite (α-Fe_2O_3), magnetite (Fe_3O_4) and/or maghemite (γ-Fe_2O_3) which show their maximum intensity reflection at 33.1°, 35.3° and 35.7°, respectively [26].

After the reaction with UV irradiation, the major presence of metallic iron was maintained in the spent nZVI/UVA particles, according to the intensity of the related XRD peaks. In addition, the new reflection peaks at 35.7°, 43.3°, 57.4°, and 63.0° indicate a significant formation of maghemite (JCPDS, No. 00-025-1402). By contrast, the sample recovered after the reaction performed with H_2O_2 and UVA irradiation (spent nZVI/H_2O_2/UVA) shows a drastic decrease in the intensity of Fe^0 signals. The concomitant appearance of new peaks, which can be ascribed to lepidocrocite (γ-FeOOH) (JCPDS, No. 01-074-1877), magnetite (JCPDS, No. 00-002-1035) and maghemite phases, certainly confirms the increased depletion of metallic iron into oxidized phases in the spent material [27].

The results obtained agree with previous works that reported the main presence of lepidocrocite, maghemite, and magnetite upon oxic corrosion of nZVI [28], namely by aging [29] or aerating the nZVI particles in aqueous solution [30]. Among the different iron phases, lepidocrocite was generally detected as the primary passivation product when the surface corrosion occurred for long periods of time, thus supporting its solely occurrence under the strongest oxidant conditions used in this work (UVA irradiation and H_2O_2 addition) in contrast to the main presence of maghemite as oxidized iron phase observed in the

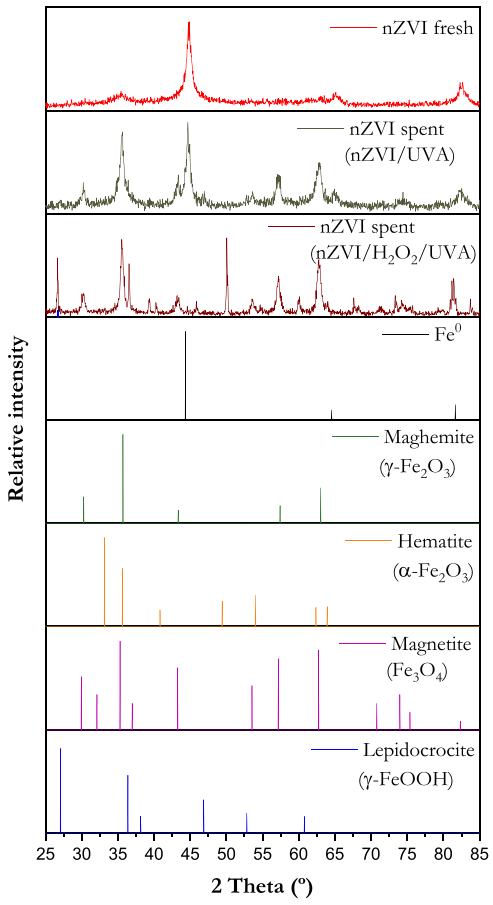

Fig. 3. XRD patterns of fresh nZVI and spent nZVI recovered after 120 min oxidation in nZVI/UVA and nZVI/H_2O_2/UVA systems. Experimental conditions: $[ATZ]_0 = 10$ mg L^{-1}; $C_{nZVI} = 0.1$ g L^{-1}; $[H_2O_2]_0 = 50$ mg L^{-1}; pH ≈ 6.3.

nZVI/UVA system.

The chemical composition changes of the nZVI particles surface were also corroborated by SEM coupled with energy dispersive X-ray (EDX) analysis (Fig. 4). Fe (red color) and O (blue color) elements are dispersed throughout the surface of pristine and spent particles, but in a different ratio. The predominance of iron in the former sample turns into a more intense contribution of O in the latter, indicating the formation of oxidized iron compounds, in agreement with the XRD results.

Fig. 5a–c displays the TEM micrographs of pristine nZVI. It shows a branched structure consisting of chains of near spherical particles of nanometric size, around 50 nm in diameter, as previously reported [29]. The particles have a core-shell structure where the core consists of metallic iron and the shell is formed by iron oxides and hydroxides, according to the energy dispersive X-ray (EDX) analysis. By contrast, the TEM images of the spent nZVI particles recovered after the reaction with H_2O_2 and UVA irradiation (Fig. 5d–f) show that the branched structure is hardly observed while there is significant aggregation of primary particles that have a smaller diameter size. Previous studies have reported that oxidation of ZVI particles occurs at the oxide-water interface under oxygen [31] and oxygenated aqueous conditions [32]. The iron oxide phase is formed on the surface after the outward diffusion of iron ions from the ZVI core to the external layer. In the presence of oxygen, Cabot et al. [31] found low-density regions in the interface iron-iron oxide attributed to the aggregation of voids created by the outward migration of iron ions. As the oxidation continues the oxide shell becomes thicker and the core is converted in a hole due to the coalescence of voids [31]. Thus, it can be inferred that the formation of void spaces in the inner part of iron nanoparticles could induce their breakthrough leading to particles with smaller diameters and mainly composed of iron oxides (Fig. 5d–f). Moreover, TEM micrographs also showed the formation of flaky and needle-shaped particles which are characteristic of lepidocrocite morphology.

Lastly, the adsorption-desorption isotherms of fresh and spent nZVI (not shown) are classified as type II with H3 type hysteresis cycle, which is referred to non-porous materials. The values of specific surface area were calculated according to the Brunauer-Emmert-Teller (BET) method. A value of 59 m^2 g^{-1} was obtained for pristine nZVI, in accordance with the range of values reported in the literature [33], whereas a decrease in the surface area to 27 m^2 g^{-1} was shown by the spent material recovered after the photo-Fenton process. This fact could be explained accounting the morphological and chemical changes of iron particles during the reaction to yield surface oxidized iron species, as described above. Although smaller particles were detected by TEM (Fig. 5f), their aggregation would lead to a decreased specific surface

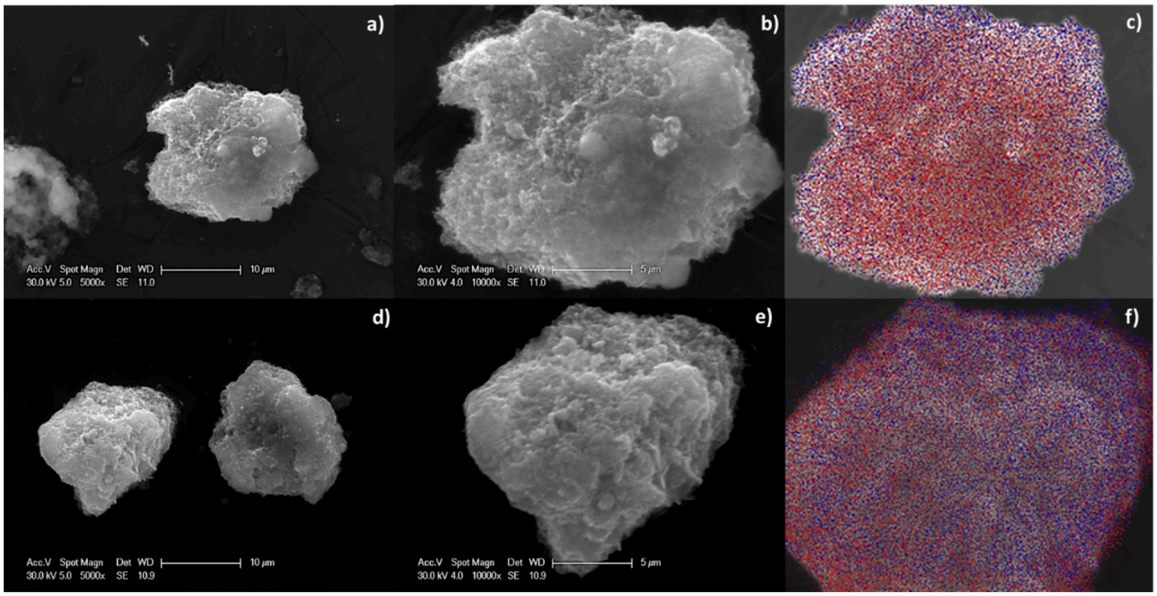

Fig. 4. SEM micrographs and EDX analysis (mapping): Fe (red) and 0 (blue) of (a–c) fresh nZVI and (d–e) spent nZVI from the reaction in the nZVI/H_2O_2/UVA system. Experimental conditions: $[ATZ]_0 = 10$ mg L^{-1}; $C_{nZVI} = 0.1$ g L^{-1}; $[H_2O_2]_0 = 50$ mg L^{-1}; pH ≈ 6.3.

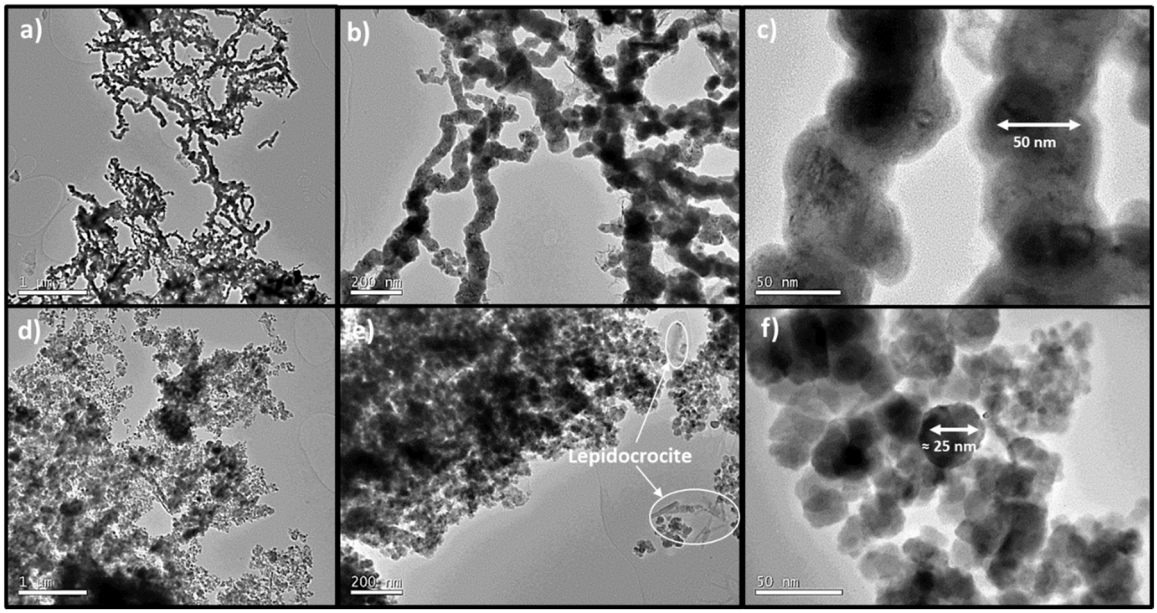

Fig. 5. TEM micrographs of fresh nZVI (a–c) and spent nZVI recovered after the reaction in the nZVI/H_2O_2/UVA system (d–f). Experimental conditions: $[ATZ]_0 = 10$ mg L^{-1}; $C_{nZVI} = 0.1$ g L^{-1}; $[H_2O_2]_0 = 50$ mg L^{-1}; pH ≈ 6.3.

area [34].

3.3. *Proposed mechanism pathway for atrazine degradation in the nZVI/H_2O_2/UVA system*

The reaction pathway of atrazine degradation was investigated by the identification and analysis of the concentration profiles of the products formed throughout 6 h in the nZVI/H_2O_2/UVA system (Figs. 6 and 7). On their basis, a mechanism summarized in Fig. 8 was proposed.

Fig. 6 shows the concentration profiles of atrazine and degradation products as a function of irradiation time (for the sake of clarity the concentration profiles of the products shown in Fig. 6a are enlarged in different Fig. 6b–d). As it can be seen, atrazine was eliminated below the detection limit after 4 h. The degradation of atrazine could be initiated by three different reactions: i) dechlorination by the attack of $HO^{\bullet}$ to the s-triazine ring at the position 2 leading to the monohydroxylated derivative EOIT (4-ethylamino-2-hydroxy-6-isopropylamino-1,3,5-triazine); ii) alkylic oxidation through the H abstraction of the secondary carbon of the alkylamino chain, forming the amide derivative; and iii) subtraction of H from the secondary carbon and introduction of an oxygen atom either by $HO^{\bullet}$ radicals or high valent oxo iron species, getting the corresponding alcohol [3,35]. The resulting products of ii) and iii) reactions can be subsequently converted in the N-dealkylated s-triazines, ACET (6-amino-2-chloro-4-ethylamino-1,3,5-triazine) and ACIT (4-amino-2-chloro-6-isopropylamino-1,3,5-triazine), maintaining the ethyl or isopropyl chain, respectively (Fig. 8).

Appreciable amounts of ACET and ACIT were found within the first 5 min of reaction (Fig. 6b), while EOIT concentration was just slightly detectable, thus suggesting that the atrazine degradation mainly started from alkylic oxidation rather than dechlorination. The prevalence of alkylic oxidation in the initial degradation pathway was also reported in a homogeneous photo-Fenton system at pH = 3, where EOIT was detected in the initial stages of reaction but in a small proportion compared to ACET and ACIT [4].

From ACET or ACIT intermediates, oxidative dealkylation could produce in both cases an amide derivative, which would be transformed to CAAT (2-chloro-4,6-diamino-1,3,5-triazine) by alkyl cleavage. As seen in Fig. 6c, CAAT was formed after 1 h of irradiation confirming the significance of this route in the mechanism. In addition, dechlorination-hydroxylation might occur simultaneously yielding AEOT (6-amino-4-ethylamino-2-hydroxy-1,3,5-triazine) from ACET as well as AOIT (4-amino-2-hydroxy-6-isopropylamino-1,3,5-triazine) from ACIT, respectively. Fig. 6b shows that while AEOT was not detected, the compound AOIT, formed after 30 min of reaction, was predominant during 4 h of reaction. It is important to remark here that AOIT can be formed not only from ACIT but also from the dechlorination-decarboxilation of other plausible intermediates such as CDIT (2-chloro-4-acetamido-6-isopropylamino-1,3,5-triazine) (Fig. 8). In addition, EOIT can be also the precursor of AOIT through the loss of the ethyl group but, if proceeds, this reaction must be very fast hence explaining that EOIT was not significantly detected in the first stage of the reaction.

The results obtained are in agreement with previous investigations on UV-Fenton degradation of ACET or ACIT as target compounds. The simultaneous dechlorination-hydroxylation and the alkylic oxidation of both, ACET and ACIT were confirmed. In addition, AOIT was also detected in a higher proportion than AEOT when atrazine was degraded [4]. Moreover, Acero et al. [36] estimated a higher rate constant of ACET degradation by ozone and/or $HO^{\bullet}$ radicals, showing the higher reactivity of the ethyl group and explaining the prevalence of isopropyl-derivative as shown here (Fig. 6c).

Both routes, through AOIT and CAAT, could converge to generate the hydroxylated products ammeline (OAAT), ammelide (OOAT) and cyanuric acid (OOOT), derived from the OH-substitution of chloride and/or amino groups (Fig. 6d). OAAT and OOAT were simultaneously observed within the first 30 min of irradiation while the detection of cyanuric acid took a longer time. Nevertheless, the concentration profiles of the three compounds with time show an increase of OAAT and OOOT concentration while, by contrast, ammelide was hardly detected after 1 h. Summarizing, after 6 h the main by-products obtained were CAAT, AOIT, OAAT, and OOOT with just slight changes in concentration of AOIT and OAAT. To better clarify the mechanism at this step, two independent runs of 7 h each were carried out using CAAT or AOIT (5 mg L^{-1}) as the starting probes. No degradation was obtained for CAAT in agreement with the results displayed in Fig. 6, which shows a steady concentration with time once the compound is formed. The resistance of CAAT indicates that this compound is not the major precursor of ammeline, since is recalcitrant in the time scale evaluated within the experimental conditions of the nZVI/H_2O_2/UVA system. A similar persistence of CAAT was found in other works regarding ATZ degradation by homogeneous Fenton at pH = 3 [3] while the

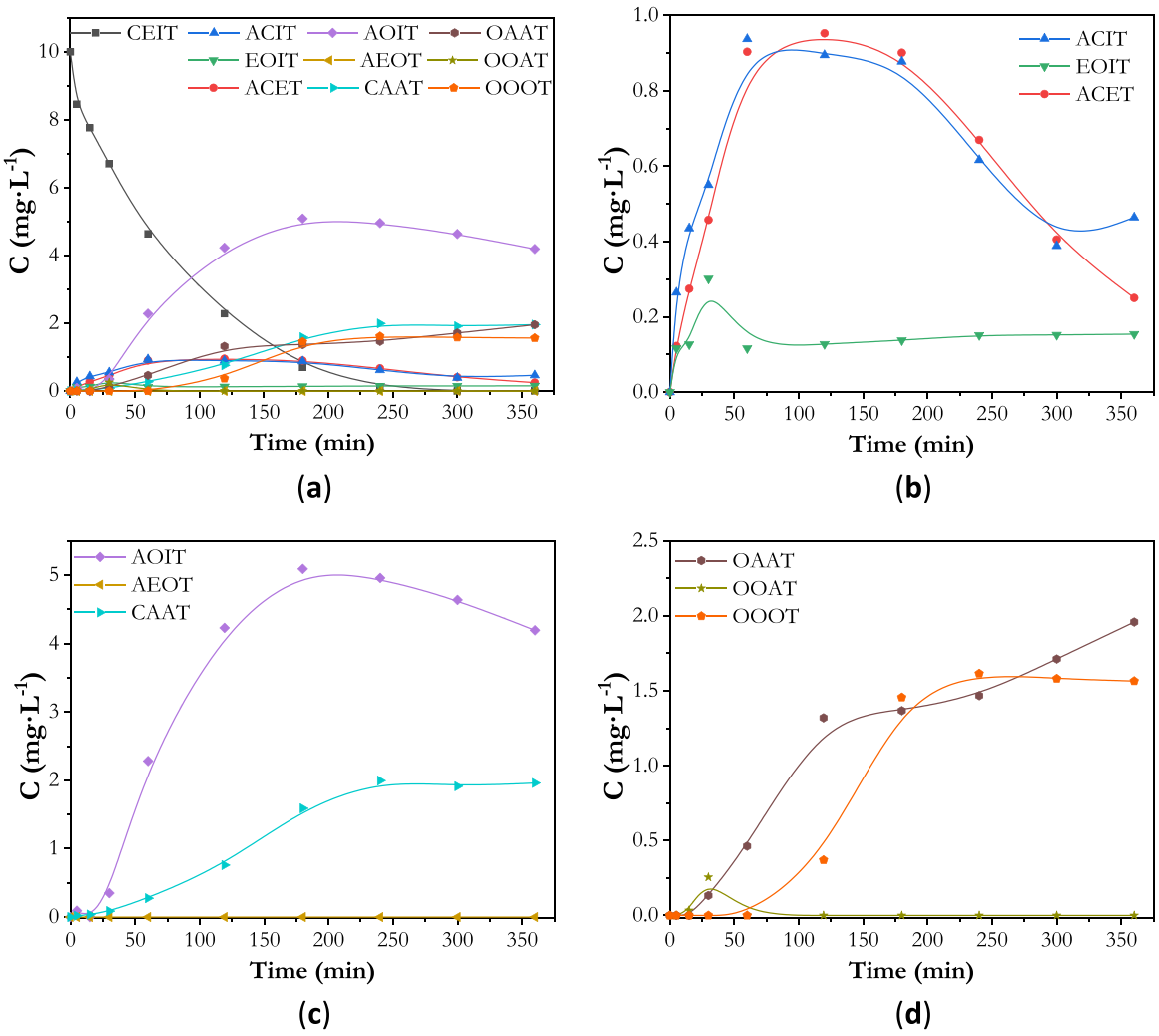

Fig. 6. (a) Concentration profiles with time of atrazine and products generated in the nZVI/H_2O_2/UVA reaction at pH ≈ 6.3. Enlargement of the evolution of (b) ACIT; EOIT; and ACET; (c) AOIT; AEOT; and CAAT; (d) OAAT; OOAT; and OOOT. Experimental conditions: $[ATZ]_0 = 10$ mg L^{-1}; $C_{nZVI} = 0.1$ g L^{-1}; $[H_2O_2]_0 = 50$ mg L^{-1}.

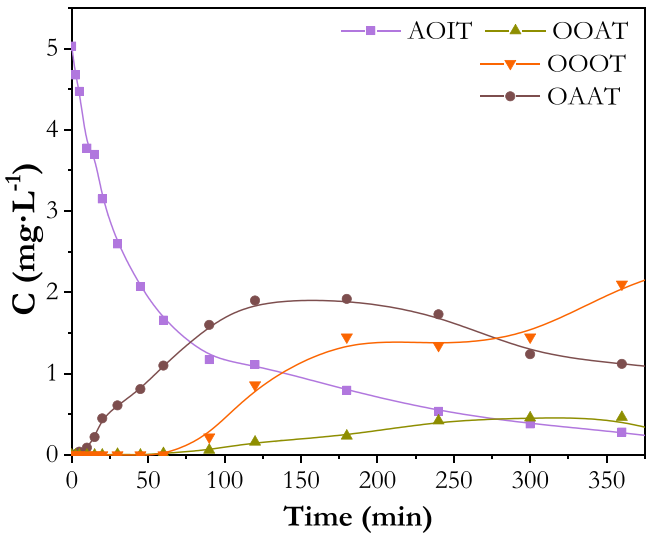

Fig. 7. Concentration profiles for AOIT degradation in the nZVI/H_2O_2/UVA system at pH ≈ 6.3. Experimental conditions: $[AOIT]_0 = 5$ mg L^{-1}; $C_{nZVI} = 0.1$ g L^{-1}; $[H_2O_2]_0 = 50$ mg L^{-1}.

degradation of the compound was achieved by homogeneous UV-photo Fenton [37], and by heterogeneous photocatalysis with TiO_2 [38,39]. However, it should be noted that a very high concentration of H_2O_2 (4000 mg L^{-1}) and large irradiation periods (> 30 h) were necessary respectively, to attain the degradation of CAAT.

By contrast, the reaction with AOIT as initial probe (Fig. 7) yielded ammeline as first degradation compound followed by cyanuric acid and ammelide as main by-products, the latter in the smaller proportion in agreement with the product distribution detected in the atrazine degradation run (Fig. 6). The comparison of concentration profiles obtained in both reactions suggests that OOAT and OOOT can be derived not only from AOIT but from other precursors such as AEOT (Fig. 8). No products resulting from the cleavage of the aromatic heterocyclic ring were observed hence being cyanuric acid the most oxidized product from atrazine degradation in the nZVI/H_2O_2/UVA system.

3.4. *Influence of the water matrix on the atrazine degradation*

It is well known that the success of a treatment for the removal of pollutants in aqueous solution strongly depends on the complexity of the water matrix since it can contain non-target species able to compete with the aimed pollutant for reactive species [40]. On this basis, the performance of the nZVI/H_2O_2/UVA system for degradation of atrazine at near circumneutral pH in different water matrixes was evaluated for:

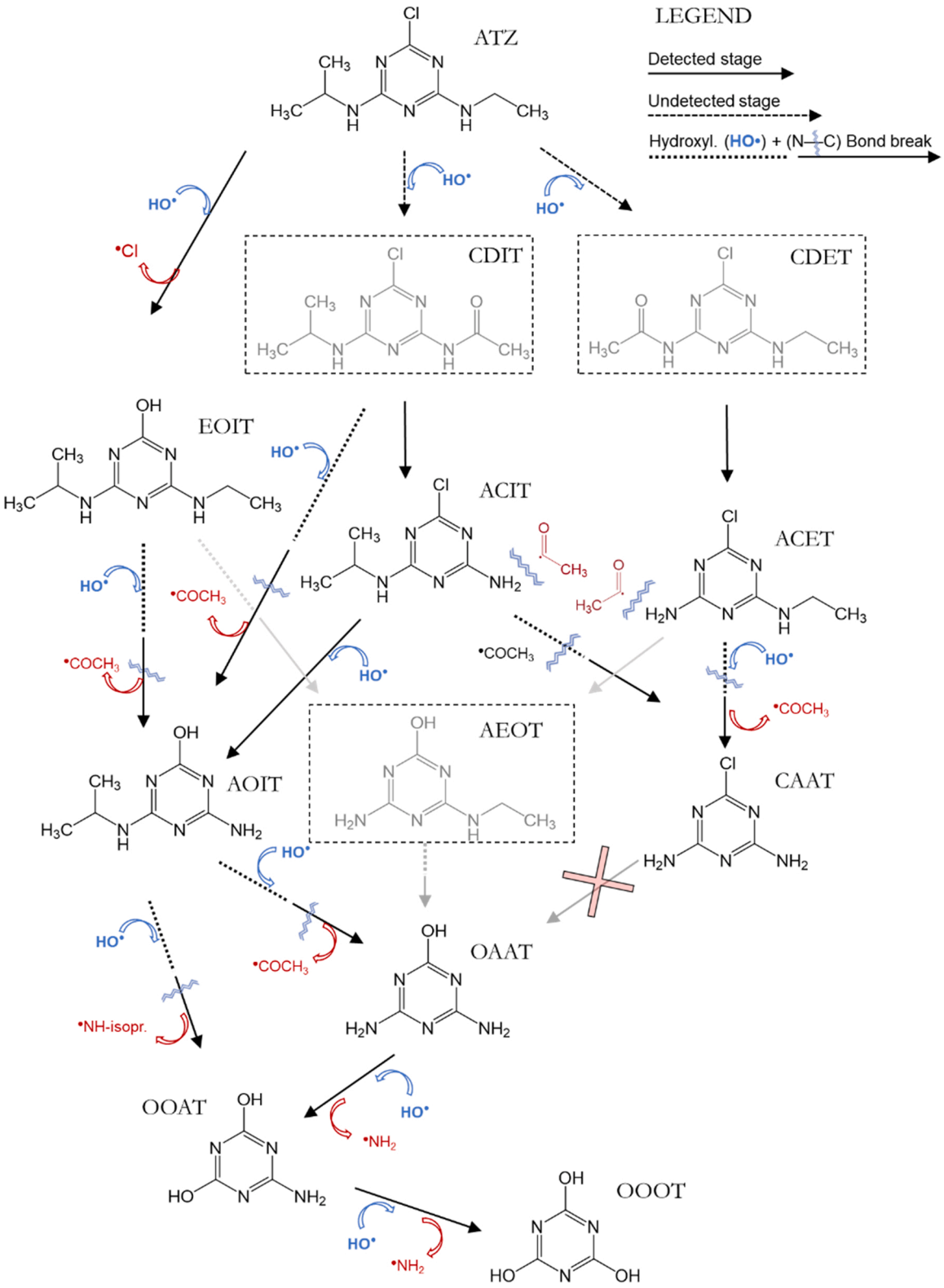

Fig. 8. Scheme proposed for atrazine degradation pathways in the nZVI/H_2O_2/UVA system.

ultrapure water (UW); public supply water obtained from the local drinking supply (PW); secondary effluent simulated water (SW); and water collected at a sewage treatment plant real secondary effluent located in Móstoles (Madrid, Spain) (RW). In all experiments 0.1 g L^{-1} nZVI and an initial 50 mg L^{-1} H_2O_2 dose were used. In agreement with previous works on photo-Fenton [41] it was evidenced (Fig. 9) a significant influence of the water matrix on the atrazine degradation rate, which was decreased following the order UW > PW > SE > RW. The kinetics were well adjusted to a pseudo-first order model obtaining k_{obs} values which ranged from 0.017 min^{-1} for UW to 0.0035 min^{-1} for RW in accordance with the increasing complexity of the water matrix.

Table 1 illustrates the main constituents of the water matrices. To

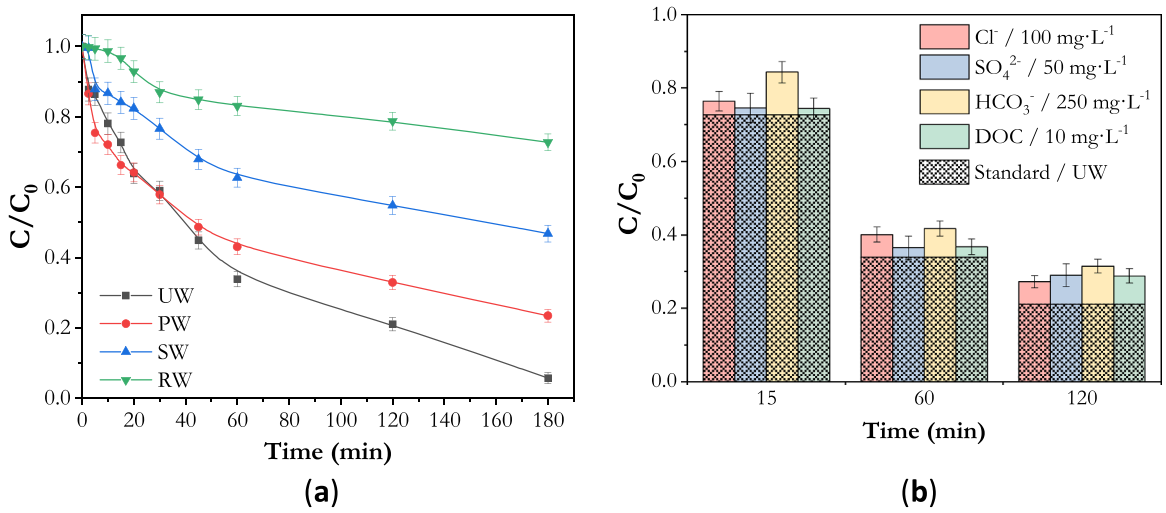

Fig. 9. Influence on atrazine degradation by nZVI/H_2O_2/UVA at pH ≈ 6.3 of (a) water matrices and (b) individual species added to PW. Experimental conditions: $[ATZ]_0 = 10$ mg L^{-1}; $C_{nZVI} = 0.1$ g L^{-1}; $[H_2O_2]_0 = 50$ mg L^{-1}.

Table 1
Concentrations in mg·L^{-1} of the main components detected in the characterization of the matrices used.

Matrix	C_{F^-}	C_{Cl^-}	$C_{NO_2^-}$	$C_{NO_3^-}$	$C_{SO_4^{2-}}$	$C_{HCO_3^-}$	C_{DOC}
UW	–	–	–	–	–	–	–
PW	0.1	34.7	0.4	2.7	21.4	62.2	2.5
SW	–	3.0	–	–	52.2	–	10.0
RW	–	150	7.9	2.8	44.0	263.0	13.3

clarify their role in the atrazine degradation kinetics, the individual effect of the most abundant, i.e. Cl^-, SO_4^{2-}, HCO_3^- and DOC, was studied by adding each species to ultrapure water in a concentration closed to that found in real water (Fig. 9b).

Compared to UW, the extent of atrazine depletion achieved after 120 min was decreased by percentages of 6.2, 7.9, 10.4, and 7.8 for Cl^-, SO_4^{2-}, HCO_3^-, and DOC, respectively, hence indicating their scavenging role as usually reported in Fenton and photo-Fenton processes. Some authors observed a positive effect of Cl^- in ZVI systems [42,43] which was explained through the acceleration of ZVI corrosion by chloride ions. However, similarly to the present work, it is generally reported a clear inhibitory effect ascribed to both the formation of $FeCl^{2+}$, which acts as a precursor of $Cl^•$ radicals in the presence of radiation [44], and the direct trapping of $HO^•$ [44,45]. The scavenging of $HO^•$ radicals has been also proposed for sulfate to form $SO_4^{•-}$ radicals, that still have a significant oxidative potential [45]. Regarding bicarbonate, in real effluents is usually found at concentrations much higher than the target compound (Table 1), therefore it can strongly compete for $HO^•$ radicals. Even though, the reaction of $HO^•$ with HCO_3^- is usually slower than $HO^•$ with the organic pollutants [46]. In addition, the longer half-life of the carbonate radical, might explain the moderate inhibition of the oxidation process despite the high bicarbonate concentration added compared to atrazine [47]. Finally, the inhibitory effect of DOC can be explained not only by its competition with atrazine for generated oxidizing radicals but also it can interfere in the irradiation of the catalyst by direct absorption of UV light [48].

Comparing the individual effect of each species (Fig. 9b) with the reactions carried out in the different matrices (Fig. 9a), it is inferred that the accumulation of the single effects, that accounts for a drop off in atrazine degradation of 32.3%, would lead to whole elimination of 46.6% that matches with the final result of SW. Moreover, a higher overall inhibition could be explained by the synergistic effects of combined anions due to reactions among formed radicals, as well as from the contribution of other species not detected in this work.

4. Conclusions

In the present work the performance of nZVI for atrazine degradation at circumneutral pH was investigated in different experimental conditions of UVA irradiation and addition of H_2O_2. In the time scale evaluated, it can be concluded that UVA irradiation of nZVI is not effective for attaining the herbicide degradation at circumneutral pH although a fast degradation of atrazine occurs in this system at acidic pH, ascribed to the in situ generation of Fenton species (H_2O_2, Fe(II) and Fe(III)).

At circumneutral conditions the addition of H_2O_2 is needed to activate the oxidative reaction with nZVI. Moreover, the UVA photo-Fenton-like process (nZVI/H_2O_2/UVA) exhibited a better performance compared to the dark nZVI/H_2O_2 system, with the production of $HO^•$ radicals being crucial for the final degradation results.

The presence of ferric oxidized species on nZVI, namely maghemite and lepidocrocite, grown in detriment of the iron core, along with the negligible concentration of iron in solution allows to confirm the heterogeneous Fenton-like mechanism initiated by the Fe(III) species and H_2O_2 and accelerated by the UVA radiation.

According to the products detected by HPLC along the reaction, it is proposed that the degradation of atrazine by nZVI/H_2O_2/UVA is mainly initiated by alkylic oxidation rather than dechlorination. In the scale of time evaluated the product CAAT is highly recalcitrant while cyanuric acid is the most oxidized product from atrazine degradation. No products resulting from the cleavage of the aromatic heterocyclic ring were observed.

The performance of the nZVI/H_2O_2/UVA system strongly depends on the water matrix. Considered individually, the main constituents of different water matrices, i.e., Cl^-, SO_4^{2-}, HCO_3^-, and DOC, showed a moderate inhibitory effect on atrazine degradation kinetics, but their combination could explain the significant decrease of efficiency detected in a real secondary effluent water compared to less complex matrices.

CRediT authorship contribution statement

Jorge Plaza: Investigation, Methodology, Writing – original draft. **Amaya Arencibia**: Investigation, Conceptualization, Supervision, Writing – review & editing. **María José López-Muñoz**: Investigation, Conceptualization, Supervision, Writing – review & editing, Funding acquisition.

Declaration of Competing Interest

The authors declare that they have no known competing financial interests or personal relationships that could have appeared to influence the work reported in this paper.

Acknowledgments

The authors gratefully acknowledge the financial support of the "Agencia Estatal de Investigación" (AEI) and the "Ministerio de Ciencia e Innovación" through the project, CALYPSOL ATECWATER (RTI2018–097997-B-C33) and to the European Union's Horizon 2020 research and innovation program under SusWater H2020-MSCA-RISE-2020 project.

References

[1] M. Graymore, F. Stagnitti, G. Allinson, Impacts of atrazine in aquatic ecosystems, Environ. Int. 26 (2001) 483–495, https://doi.org/10.1016/S0160-4120(01)00031-9.
[2] The European Parlament and the Council of the European Union, Directives of 12 August 2013 amending Directives 2000/60/EC and 2008/105/EC as regards priority substances in the field of water policy, Off. J. Eur. Union, 2013, pp. 1–17. ⟨https://doi.org/http://eur-lex.europa.eu/legal-content/EN/TXT/?uri=celex:32013L0039⟩.
[3] S.M. Arnold, W.J. Hickey, R.F. Harris, Degradation of atrazine by Fenton's reagent: condition optimization and product quantification, Environ. Sci. Technol. 29 (1995) 2083–2089, https://doi.org/10.1021/es00008a030.
[4] K.H. Chan, W. Chu, Model applications and intermediates quantification of atrazine degradation by UV-enhanced fenton process, J. Agric. Food Chem. 54 (2006) 1804–1813, https://doi.org/10.1021/jf052572e.
[5] T.B. Benzaquén, M.A. Isla, O.M. Alfano, Fenton and photo-Fenton processes for the degradation of atrazine: a kinetic study, J. Chem. Technol. Biotechnol. 90 (2015) 459–467, https://doi.org/10.1002/jctb.4324.
[6] E.G. Garrido-Ramírez, B.K.G. Theng, M.L. Mora, Clays and oxide minerals as catalysts and nanocatalysts in Fenton-like reactions – a review, Appl. Clay Sci. 47 (2010) 182–192, https://doi.org/10.1016/j.clay.2009.11.044.
[7] R.M. Cornell, U. Schwertmann, The Iron Oxides, Wiley, 2003, https://doi.org/10.1002/3527602097.
[8] F. Fu, D.D. Dionysiou, H. Liu, The use of zero-valent iron for groundwater remediation and wastewater treatment: a review, J. Hazard. Mater. 267 (2014) 194–205, https://doi.org/10.1016/j.jhazmat.2013.12.062.
[9] I. De La Obra, B. Esteban García, J.L. García Sánchez, J.L. Casas López, J.A.S.á nchez Pérez, Low cost UVA-LED as a radiation source for the photo-Fenton process: a new approach for micropollutant removal from urban wastewater, Photochem. Photobiol. Sci. 16 (2017) 72–78, https://doi.org/10.1039/c6pp00245e.
[10] S.M. Ponder, J.G. Darab, T.E. Mallouk, Remediation of Cr(VI) and Pb(II) aqueous solutions using supported, nanoscale zero-valent iron, Environ. Sci. Technol. 34 (2000) 2564–2569, https://doi.org/10.1021/es9911420.
[11] T. Harada, T. Yatagai, Y. Kawase, Hydroxyl radical generation linked with iron dissolution and dissolved oxygen consumption in zero-valent iron wastewater treatment process, Chem. Eng. J. 303 (2016) 611–620, https://doi.org/10.1016/j.cej.2016.06.047.
[12] H.J. Sung, A.J. Feitz, D.L. Sedlak, T.D. Waite, Quantification of the oxidizing capacity of nanoparticulate zero-valent iron, Environ. Sci. Technol. 39 (2005) 1263–1268, https://doi.org/10.1021/es048983d.
[13] S.J. Hug, O. Leupin, Iron-catalyzed oxidation of arsenic(III) by oxygen and by hydrogen peroxide: pH-dependent formation of oxidants in the Fenton reaction, Environ. Sci. Technol. 37 (2003) 2734–2742, https://doi.org/10.1021/es026208x.
[14] C.R. Keenan, D.L. Sedlak, Factors affecting the yield of oxidants from the reaction of nanonarticulate zero-valent iron and oxygen, Environ. Sci. Technol. 42 (2008) 1262–1267, https://doi.org/10.1021/es7025664.
[15] H.S. Son, J.K. Im, K.D. Zoh, A Fenton-like degradation mechanism for 1,4-dioxane using zero-valent iron (Fe0) and UV light, Water Res. 43 (2009) 1457–1463, https://doi.org/10.1016/j.watres.2008.12.029.
[16] I. Grčić, S. Papić, K. Žižek, N. Koprivanac, Zero-valent iron (ZVI) Fenton oxidation of reactive dye wastewater under UV-C and solar irradiation, Chem. Eng. J. 195–196 (2012) 77–90, https://doi.org/10.1016/j.cej.2012.04.093.
[17] S.H. Joo, A.J. Feitz, T.D. Waite, Oxidative degradation of the carbothioate herbicide, molinate, using nanoscale zero-valent iron, Environ. Sci. Technol. 38 (2004) 2242–2247, https://doi.org/10.1021/es035157g.
[18] X. Sun, T. Kurokawa, M. Suzuki, M. Takagi, Y. Kawase, Removal of cationic dye methylene blue by zero-valent iron: effects of pH and dissolved oxygen on removal mechanisms, J. Environ. Sci. Heal. - Part A Toxic Hazard. Subst. Environ. Eng. 50 (2015) 1057–1071, https://doi.org/10.1080/10934529.2015.1038181.
[19] N. Fujioka, M. Suzuki, S. Kurosu, Y. Kawase, Linkage of iron elution and dissolved oxygen consumption with removal of organic pollutants by nanoscale zero-valent iron: effects of pH on iron dissolution and formation of iron oxide/hydroxide layer, Chemosphere 144 (2016) 1738–1746, https://doi.org/10.1016/j.chemosphere.2015.10.064.
[20] S. Giannakis, M.I. Polo López, D. Spuhler, J.A. Sánchez Pérez, P. Fernández Ibáñez, C. Pulgarin, Solar disinfection is an augmentable, in situ-generated photo-Fenton reaction—part 1: a review of the mechanisms and the fundamental aspects of the process, Appl. Catal. B Environ. 199 (2016) 199–223, https://doi.org/10.1016/j.apcatb.2016.06.009.
[21] C. Ruales-Lonfat, J.F. Barona, A. Sienkiewicz, M. Bensimon, J. Vélez-Colmenares, N. Benítez, C. Pulgarín, Iron oxides semiconductors are efficients for solar water disinfection: a comparison with photo-Fenton processes at neutral pH, Appl. Catal. B Environ. 166–167 (2015) 497–508, https://doi.org/10.1016/j.apcatb.2014.12.007.
[22] S.S. Lin, M.D. Gurol, Catalytic decomposition of hydrogen peroxide on iron oxide: Kinetics, mechanism, and implications, Environ. Sci. Technol. 32 (1998) 1417–1423, https://doi.org/10.1021/es970648k.
[23] R. Andreozzi, A. D'Apuzzo, R. Marotta, Oxidation of aromatic substrates in water/goethite slurry by means of hydrogen peroxide, Water Res. 36 (2002) 4691–4698, https://doi.org/10.1016/S0043-1354(02)00204-X.
[24] J. He, X. Tao, W. Ma, J. Zhao, Heterogeneous photo-Fenton degradation of an azo dye in aqueous H2O2/iron oxide dispersions at neutral pHs, Chem. Lett. 31 (2002) 86–87, https://doi.org/10.1246/cl.2002.86.
[25] M. Li, Z. Qiang, C. Pulgarin, J. Kiwi, Accelerated methylene blue (MB) degradation by Fenton reagent exposed to UV or VUV/UV light in an innovative micro photo-reactor, Appl. Catal. B Environ. 187 (2016) 83–89, https://doi.org/10.1016/j.apcatb.2016.01.014.
[26] Y.P. Sun, X. qin Li, J. Cao, W. xian Zhang, H.P. Wang, Characterization of zero-valent iron nanoparticles, Adv. Colloid Interface Sci. 120 (2006) 47–56, https://doi.org/10.1016/j.cis.2006.03.001.
[27] G.C. Allen, M.T. Curtis, A.J. Hooper, P.M. Tucker, X-Ray photoelectron spectroscopy of iron-oxygen systems, J. Chem. Soc. Dalton Trans. (1974) 1525–1530, https://doi.org/10.1039/DT9740001525.
[28] S. Bae, R.N. Collins, T.D. Waite, K. Hanna, Advances in surface passivation of nanoscale zerovalent iron: a critical review, Environ. Sci. Technol. 52 (2018) 12010–12025, https://doi.org/10.1021/acs.est.8b01734.
[29] A. Liu, J. Liu, W. xian Zhang, Transformation and composition evolution of nanoscale zero valent iron (nZVI) synthesized by borohydride reduction in static water, Chemosphere 119 (2015) 1068–1074, https://doi.org/10.1016/j.chemosphere.2014.09.026.
[30] D. He, J. Ma, R.N. Collins, T.D. Waite, Effect of structural transformation of nanoparticulate zero-valent iron on generation of reactive oxygen species, Environ. Sci. Technol. 50 (2016) 3820–3828, https://doi.org/10.1021/acs.est.5b04988.
[31] A. Cabot, V.F. Puntes, E. Shevchenko, Y. Yin, L. Balcells, M.A. Marcus, S. M. Hughes, A.P. Alivisatos, Vacancy coalescence during oxidation of iron nanoparticles, J. Am. Chem. Soc. 129 (2007) 10358–10360, https://doi.org/10.1021/ja072574a.
[32] L.F. Greenlee, J.D. Torrey, R.L. Amaro, J.M. Shaw, Kinetics of zero valent iron nanoparticle oxidation in oxygenated water, Environ. Sci. Technol. 46 (2012) 12913–12920, https://doi.org/10.1021/es303037k.
[33] Y. Xi, M. Mallavarapu, R. Naidu, Reduction and adsorption of Pb2+ in aqueous solution by nano-zero-valent iron – a SEM, TEM and XPS study, Mater. Res. Bull. 45 (2010) 1361–1367, https://doi.org/10.1016/j.materresbull.2010.06.046.
[34] A.M.E. Khalil, O. Eljamal, R. Eljamal, Y. Sugihara, N. Matsunaga, Treatment and regeneration of nano-scale zero-valent iron spent in water remediation, Evergreen 4 (2017) 21–28, https://doi.org/10.5109/1808449.
[35] K.H. Chan, W. Chu, Model applications and mechanism study on the degradation of atrazine by Fenton's system, J. Hazard. Mater. 118 (2005) 227–237, https://doi.org/10.1016/j.jhazmat.2004.11.008.
[36] J.L. Acero, K. Stemmler, U. Von Gunten, Degradation kinetics of atrazine and its degradation products with ozone and OH radicals: a predictive tool for drinking water treatment, Environ. Sci. Technol. 34 (2000) 591–597, https://doi.org/10.1021/es990724e.
[37] S. Dbira, A. Bedoui, N. Bensalah, Investigations on the degradation of triazine herbicides in water by photo-Fenton process, Am. J. Anal. Chem. 05 (2014) 500–517, https://doi.org/10.4236/ajac.2014.58059.
[38] M.J. López-Muñoz, J. Aguado, A. Revilla, Photocatalytic removal of s-triazines: evaluation of operational parameters, Catal. Today 161 (2011) 153–162, https://doi.org/10.1016/j.cattod.2010.10.076.
[39] H. Krýsová, J. Jirkovský, J. Krýsa, G. Mailhot, M. Bolte, Comparative kinetic study of atrazine photodegradation in aqueous Fe(ClO4)3 solutions and TiO2 suspensions, Appl. Catal. B Environ. 40 (2003) 1–12, https://doi.org/10.1016/S0926-3373(01)00324-1.
[40] A.R. Lado Ribeiro, N.F.F. Moreira, G. Li Puma, A.M.T. Silva, Impact of water matrix on the removal of micropollutants by advanced oxidation technologies, Chem. Eng. J. 363 (2019) 155–173, https://doi.org/10.1016/j.cej.2019.01.080.
[41] L. Santos-Juanes, R.F. Vercher, A.M. Amat, A. Arques, S. García-Ballesteros, R. F. Vercher, A.M. Amat, A. Arques, Commercial steel wool used for zero valent iron and as a source of dissolved iron in a combined red-ox process for pentachlorophenol degradation in tap water, Catal. Today 328 (2019) 252–258, https://doi.org/10.1016/j.cattod.2019.01.007.
[42] J.A. de Lima Perini, R.F.P. Nogueira, Effect of particle size, iron ligands and anions on ciprofloxacin degradation in zero-valent iron process: application to sewage treatment plant effluent, J. Chem. Technol. Biotechnol. 92 (2017) 2300–2308, https://doi.org/10.1002/jctb.5227.
[43] R. Ling, J.P. Chen, J. Shao, M. Reinhard, Degradation of organic compounds during the corrosion of ZVI by hydrogen peroxide at neutral pH: kinetics, mechanisms and effect of corrosion promoting and inhibiting ions, Water Res 134 (2018) 44–53, https://doi.org/10.1016/j.watres.2018.01.065.

[44] J. Soler, A. García-Ripoll, N. Hayek, P. Miró, R. Vicente, A. Arques, A.M. Amat, Effect of inorganic ions on the solar detoxification of water polluted with pesticides, Water Res. 43 (2009) 4441–4450, https://doi.org/10.1016/j.jhazmat.2011.01.089.
[45] A. Zapata, I. Oller, E. Bizani, J.A. Sánchez-Pérez, M.I. Maldonado, S. Malato, Evaluation of operational parameters involved in solar photo-Fenton degradation of a commercial pesticide mixture, Catal. Today 144 (2009) 94–99, https://doi.org/10.1016/j.cattod.2008.12.030.
[46] G.V. Buxton, C.L. Greenstock, W.P. Helman, A.B. Ross, Critical review of rate constants for reactions of hydrated electrons, hydrogen atoms and hydroxyl radicals (·OH/·O⁻ in aqueous solution, J. Phys. Chem. Ref. Data 17 (1988) 513–886, https://doi.org/10.1063/1.555805.
[47] C.A.L. Graça, L.T.N. Fugita, A.C. de Velosa, A.C.S.C. Teixeira, Amicarbazone degradation promoted by ZVI-activated persulfate: study of relevant variables for practical application, Environ. Sci. Pollut. Res. 25 (2018) 5474–5483, https://doi.org/10.1007/s11356-017-0862-9.
[48] L. Haroune, M. Salaun, A. Ménard, C.Y. Legault, J.P. Bellenger, Photocatalytic degradation of carbamazepine and three derivatives using TiO2 and ZnO: effect of pH, ionic strength, and natural organic matter, Sci. Total Environ. 475 (2014) 16–22, https://doi.org/10.1016/j.scitotenv.2013.12.104.